PROCEEDINGS OF THE ROYAL SOCIETY A MATHEMATICAL, PHYSICAL & ENGINEERING SCIENCES

The Effect of Initial Diameter in Spherically Symmetric Droplet Combustion of Sooting Fuels

G. S. Jackson and C. T. Avedisian

Proc. R. Soc. Lond. A 1994 **446**, doi: 10.1098/rspa.1994.0103, published 8 August 1994

The effect of initial diameter in spherically symmetric droplet combustion of sooting fuels†

By G. S. Jackson‡ and C. T. Avedisian

Sibley School of Mechanical and Aerospace Engineering, Cornell University, Ithaca, New York 14853, U.S.A.

The effect of initial droplet diameter on the burning rate of sooting fuels – n-heptane and 1-chloro-octane – was examined experimentally at low gravity. A 1.2 s drop tower provided a low gravity environment to minimize buoyancy and achieve spherically symmetric flames for stationary droplets. Free-floating and fibre-supported droplets were burned, and both techniques gave matching results for droplets of similar initial diameter. Burning rate constants for both fuels were measured for a large number of droplets ranging from 0.4 to 1.1 mm in initial diameter.

Results showed that burning rate constants decreased monotonically as the initial droplet diameter was increased above 0.6 mm for both fuels. This decrease was considered to be due to the observed increase in soot formation and accumulation in a shell-like structure inside the flame of the larger droplets. The increased collection of soot inside the larger droplet flames reduced the proportional heat release from the flame and may have acted as a barrier to heat transfer from the flame to the droplet. Flame-to-droplet diameter ratio increased monotonically with time, thus suggesting that quasi-steady combustion was not achieved. The flames and soot shells for 1-chloro-octane droplets with their lower burning rates remained closer to the droplet surface than similarly sized n-heptane droplets.

1. Introduction

The various approximations that form the basis of the classical theory of spherically symmetric droplet combustion as pioneered by Spalding (1953) combine to yield a burning rate, K_0, defined as

$$d^2 = d_0^2 - K_0 t \tag{1.1}$$

(d is the droplet diameter at time t and d_0 is the initial diameter just before ignition), which is independent of d_0. Furthermore, the variation of the ratio of the droplet diameter with the flame diameter, d_f, is a constant

$$d_f/d = \text{const.} \tag{1.2}$$

† This paper was produced from the authors' disk by using the TEX typesetting system.

‡ Present address: Precision Combustion, Inc., New Haven, Connecticut 06511, U.S.A.

Proc. R. Soc. Lond. A (1994) **446**, 255–276
Printed in Great Britain

The above two results constitute the so-called 'quasi-steady' theory of droplet combustion (Williams 1973, 1985). As an aside, (1.1) is apparently satisfied in many situations whereas past experimental observations (Okajima & Kumagai 1975) have suggested that (1.1) is not. While the quasi-steady result has undergone several extensions to include such effects as transient liquid-phase heating (Law 1976), gas-phase fuel vapour accumulation (Matalon & Law 1985), and variable gas-phase transport properties (Puri & Libby 1991), these improved models have also predicted burning rate constants in the final quasi-steady burning régime which were basically independent of droplet diameter.

However, measurements of the evolution of droplet diameter in the spherically symmetric (microgravity) configuration suggest that K_0 may in fact be dependent on d_0, at least for fuels that produce soot (Jackson *et al.* 1992). The evidence centres around the differing burning rates reported for droplets of different initial diameter of the same fuel. An explanation could reside in the dependence of droplet diameter on soot formation. In the case of a droplet experiencing a shear force at its surface, experimental evidence shows that soot formation increases as the droplet diameter increases (Kesten *et al.* 1980). The present study looks more closely at this issue for the spherically symmetric case.

Soot formation processes cannot be incorporated in a model for droplet combustion which uses the flame sheet approximation, and the few studies which have relaxed this assumption for spherically symmetric burning (Card & Williams 1992; Cho *et al.* 1990) have not yet included the great complexities associated with soot reaction mechanisms. If soot formation during droplet combustion significantly influences the burning rate, then the burning rate constant may not be single valued even under conditions of spherically symmetric combustion. The recent experimental results of spherically symmetric combustion of n-heptane, in particular, show a variation in K_0 with initial droplet diameter which is not accounted for by the classical theory.

The present experimental study was undertaken to help resolve the issue of a possible effect of droplet diameter on the spherically symmetric burning rate. The experiment was designed with a view toward the assumptions of the quasi-steady theory. These include (Williams 1985): (1) spherical symmetry, (2) isolated droplet, (2) ignition symmetry, and (4) quiescent ambience. However, the simplicity of the spherically symmetric configuration belies the difficulty of constructing an experiment which conforms to the model assumptions. Recent work, though, has extended the earlier efforts of Okajima & Kumagai (1975) in this regard (Avedisian *et al.* 1988; Hara & Kumagai 1990; Choi *et al.* 1990; Jackson *et al.* 1991, 1992).

Data from both free-floating droplets and droplets suspended from a relatively thin support fibre are reported here. Fibre supported droplets are relatively simple to study because the droplets are fixed at a location where they can be imaged throughout the burning process. However, the fibre can affect the burning process in a variety of ways. To ensure that the fibre was not artificially influencing the burning process, results from fibre supported droplets were compared with data obtained from free-floating droplets burning under the same ambient conditions. On the other hand, it is more difficult to create near stationary and free-floating droplets in microgravity in part because any slight movement of the droplets can cause them to drift out of the field of view.

Two fuels were examined in the present study: n-heptane (C_7H_{16}) and 1-chloro-

octane ($C_8H_{17}Cl$). N-heptane represented a lightly sooting fuel, and 1-chlorooctane represented a highly-sooting fuel that characterizes the behaviour of chlorinated hazardous waste incinerator feed stocks. Many droplets for both fuels were burned in a room temperature ambience under conditions of low or negligible buoyancy to assess the effect of droplet size upon K_0. Although the composition of inert gas in an ambience of fixed oxygen concentration may influence the spherically symmetric droplet burning rate (Choi *et al.* 1993), for the experiments reported here the ambience was air to avoid complicating the interpretation of the effect of initial diameter on the droplet burning rate. Spherically symmetric burning was promoted by performing the experiments in microgravity. The initial droplet diameters of both the fibre supported and free-floating droplets ranged from 0.4 mm to about 1 mm.

2. Effect of diameter on the convective droplet burning rate

While the present study focuses on the spherically symmetric droplet burning rate and its dependence on initial droplet diameter, K_0 can also be an important value for predicting the burning rate of a droplet in a convective environment.

In combustion devices such as diesel engines, industrial furnaces, spray-fired incinerators, etc., droplets are invariably moving when they burn. Convective flows distort the flame from a spherical shape and alter the rate of heat transferred from the exothermic reactions in the gas-phase to the droplet surface. The burning rate constant then becomes a function of the intensity of the convective flows. Dimensionless parameters that characterize the intensity of these flows include the Grashof (or more precisely the Rayleigh) number for natural convection which varies as d^3, and the Reynolds number for forced convection which varies as d.

Predictions of the convective droplet burning rate are often based on a simplified form that treat the burning rate as a perturbation of the spherically symmetric value:

$$K = K_0(1 + aRe_d^b)(1 + cGr_d^f), \tag{2.1}$$

where Re and Gr are the Reynolds and Grashof numbers, respectively, based on the droplet diameter d. Equation (2.1) formally applies in the limit of a Stokesian flow where $Gr = 0$ (Fendell *et al.* 1966; Gogos *et al.* 1986) though it is often used even when far from this limit (Law & Williams 1972). The addition of the term with Gr is *ad hoc*. The consistency of (2.1) is dependent somewhat on the limiting form for K being recovered when $Re \to 0$ and $Gr \to 0$, since then $K \to K_0$. The empirically determined constants a, b, c and f can certainly depend on the choice of K_0. Theory shows that when $Gr = 0$, $c = \frac{1}{2}$ and $a = \frac{1}{2}$ (Gogos *et al.* 1986) regardless of K_0.

Equation (2.1) suggests that K should decrease as the droplet diameter decreases. A trend of decreasing burning rate with decreasing droplet diameter in a convective environment has been verified experimentally (Monaghan *et al.* 1968).

3. Experimental

(*a*) *Technique*

To promote spherically symmetric droplet combustion conditions, experiments were conducted in microgravity on board a freely falling package. The instrumen-

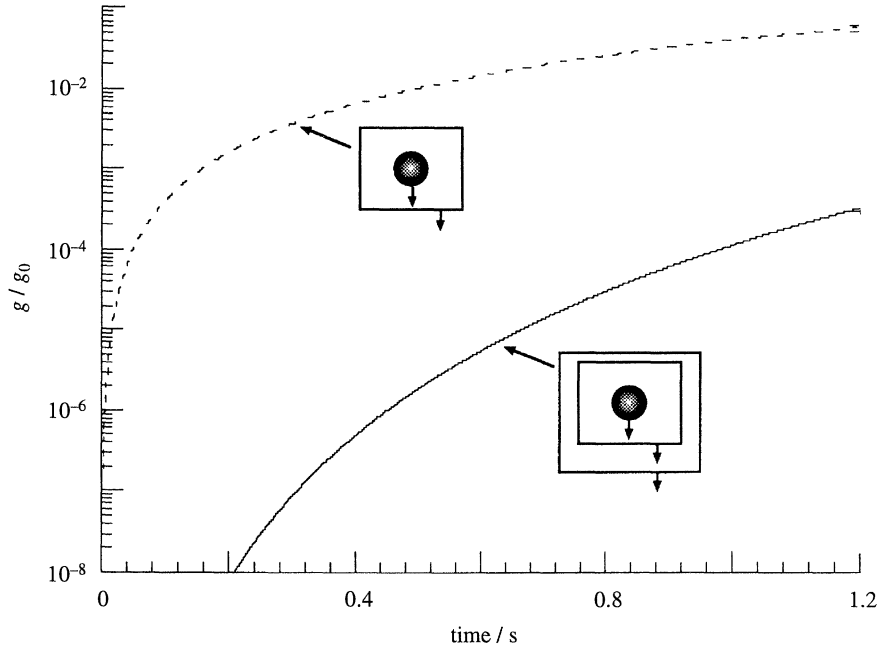

Figure 1. Evolution of gravity (calculated) in the moving frame of reference with and without a drag shield; $g_0 \approx 9.8$ m s^{-1}.

tation package was allowed to fall freely within a larger outer package – a drag shield – to minimize air drag on the package and a consequence rise in gravity on board the instrumentation package. Figure 1 illustrates the calculated (Jackson 1994) evolution of gravity in the moving frame of reference by applying a force balance on the package falling inside the simultaneously falling drag shield. For comparison, calculated gravity levels for an unshielded falling package are shown as well. The curve for the unshielded package compares favorably with accelerometer measurements reported previously (Avedisian *et al.* 1988). Figure 1 shows that the outer shield reduced the gravity level by more than an order of magnitude.

The use of a drag shield was particularly necessary for maintaining spherical flames around the larger droplets reported here – droplets with an initial diameter larger than about 1 mm – because these droplets burned for the entire period of free-fall of the instrumentation package. Flame shapes surrounding droplets of this size were spherical up to the moment of impact of the shielded package. On the other hand, the effective gravity of an unshielded package was large enough to create significant buoyant flows around such droplets to distort the flame shape well before impact (typically after around 0.5 s after release of the instrumentation package). For droplets with initial diameters around 0.5 mm, the burning times were short enough for the burning process to be completed before significant buoyant flows could develop, thus causing the flame to become non-spherical (Jackson *et al.* 1992). The use of a drag shield would then have no effect on the result.

The instrumentation package contained a combustion chamber in which was mounted the droplet generator and ignition source. The instrumentation package

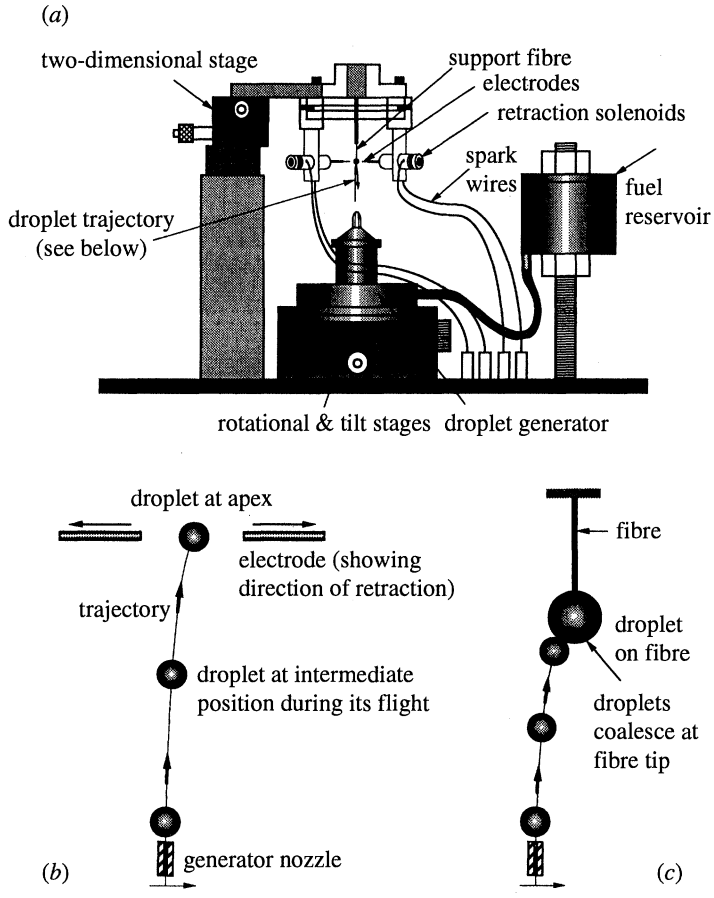

Figure 2. (*a*) Droplet generator with electrode mount. (*b*) Illustration of free droplet arrangement. (*c*) 'Shooting' method for forming a small droplet on a fibre.

also contained appropriate back lighting for the droplet, a high-speed movie camera to obtain film records for data extraction, and a light-sensitive CCD camera mounted at a right angle to the movie camera. The CCD camera provided for good visualization of the flame surrounding the droplet. Care was taken to purge the combustion chamber with air just before performing each experiment.

Two techniques were used to observe the combustion of stationary isolated droplets: free unsupported droplets and fibre-supported droplets. The technique for creating free or unsupported droplets has been described previously (Avedisian *et al.* 1988; Jackson *et al.* 1991, 1992). Briefly, a droplet generator (figure 2*a*) propelled droplets in a near vertical trajectory, and when the droplets reached the apex of their flight the package was released into free fall such that the droplet and the camera fell simultaneously. Figure 2*b* illustrates this operation. The initial size of the droplets was controlled by varying the orifice diameter of the droplet generator nozzle.

Droplets as small as 0.5 mm in diameter were deposited onto a fibre by placing the beaded tip of the quartz fibre at the apex of the droplet trajectory (figure 2*b*) so that a droplet would hit the fibre tip as shown in figure 2*c*. A wide range of

droplet sizes could be deposited onto the fibre with this method by essentially allowing several droplets to hit and coalesce at the fibre tip. The fibre diameter was about 30 μm except for the largest supported droplets studied (*ca.* 1.0 mm diameter) for which fibres with diameters of about 50 μm were used. The corresponding bead diameter was about twice the fibre diameter. Easy transfer between the two types of experimental configurations – free droplets and supported droplets – was possible with this arrangement.

The most extensive data obtained from the experiments was the evolution of the droplet diameter during combustion. Additional measurements were made for the flame diameter. Only films in sharp focus, with very low convective velocities, and which recorded a significant fraction of the total droplet burning time were accepted for analysis to be able to distinguish small (*ca.* 10%) variations in the burning rate constants. The burning rates for fibre-supported droplets matched the burning rates of free or unsupported droplets of similar size. Differences in burning rates of similar-sized n-heptane droplets between the fibre supported and free floating droplets were well within uncertainty for the entire range of initial diameters for the two droplet configurations. This fact indicates that the fibre had a negligible effect on the burning rate as further discussed in § 4. Due to the shorter set-up time and lower vapour production of the suspended droplet technique relative to the unsupported droplet method used, all 1-chloro-octane droplets were burned as suspended droplets to minimize possible health hazards.

The droplets were ignited by two electric sparks (requiring four electrodes) symmetrically positioned on opposite sides of the droplet. For the unsupported droplets, the electrodes were positioned at the apex of the droplet trajectory. The two sparks were generated simultaneously between two 0.2 mm diameter stainless steel electrode tips placed between 3 and 5 mm apart from each other as schematically illustrated in figure 3. The sparks were created by a microsecond high voltage inductive breakdown followed by a relatively low voltage high current capacitive discharge. The circuit allowed for control of the spark current, voltage, and duration to control the energy. A full description of the spark circuitry is discussed in Jackson (1994). The spark duration was kept as low as possible for achieving ignition because previous experiments (Jackson *et al.* 1992) indicated that longer sparks enhanced soot formation in the early period of the droplet burning lifetime. The spark energy, provided primarily by the capacitance discharge, was also kept near the minimum required for ignition, to reduce droplet oscillations from the discharge after ignition. In the experiments reported here for n-heptane, the spark duration was 0.5 ms and the spark energy was around 0.03 J. The less volatile chloro-octane required much longer spark durations (from 4 to 11 ms) and higher energy levels (around 0.4 J to around 0.7 J). The highest energy levels were required for droplets with initial diameters larger than around 0.8 mm.

After ignition, the electrodes were retracted in the direction shown in figure 2*b* by making part of the electrodes out of 1.6 mm diameter ferromagnetic steel rods such that they could be moved rather like a solenoid plunger. The electrodes freely floated in a sleeve which had a solenoid coil around one section. The electrodes made a brushing contact with the spark wires which were fed into the sleeve at right angles to the movement of the electrodes. This arrangement, which is shown in the enlargement of figure 3, minimized air disturbances from the electrode

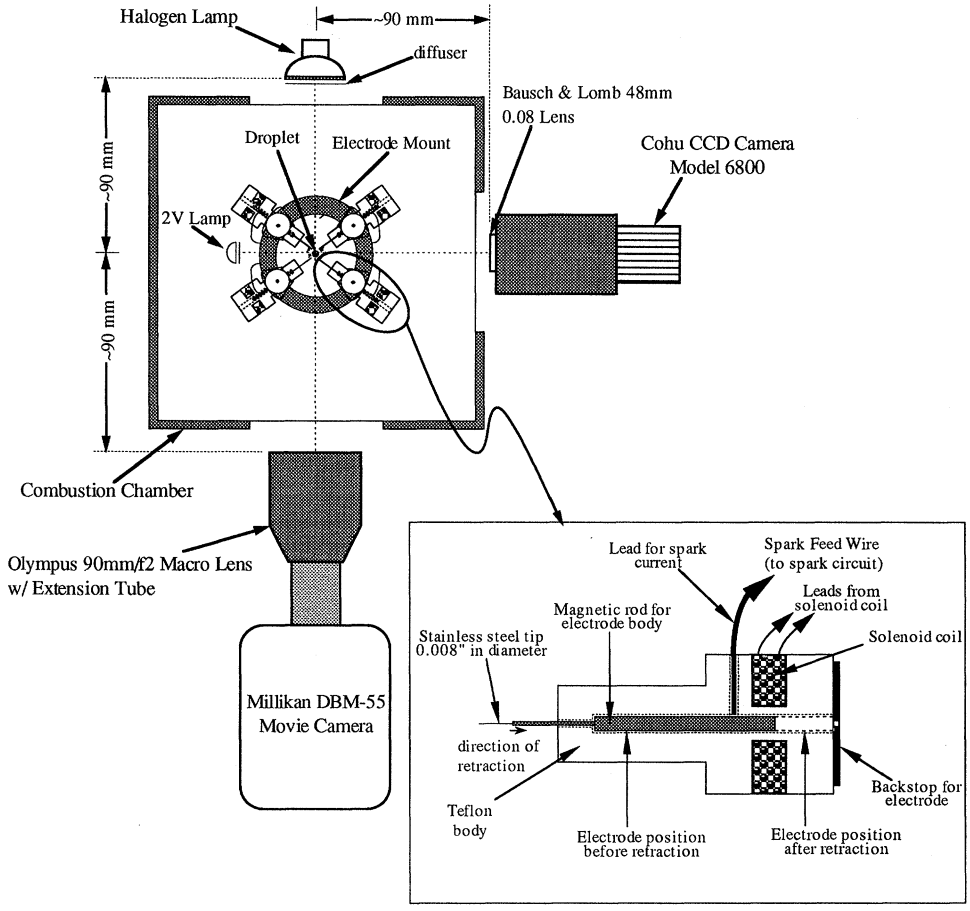

Figure 3. Layout of optical arrangement on board the experimental package. Enlargement shows details of electrode and solenoid for retraction.

retraction since only the electrodes themselves were required to move radially outward.

(*b*) *Data reduction*

Droplet and flame diameter measurements were obtained from the high-speed movie records through a frame-by-frame analyses using a computer based image analyses system (Image Analyst^{TM}, Automatix Inc., Billerica, MA). Framing rates ranged from 100 frames per second for the larger droplets to 250 frames per second for the smaller, faster burning, droplets. The image analysis program calculated an average droplet diameter by finding a perimeter with a threshold grey level which was set according to the background of the film around the droplet, and averaging the distances from the centroid to the perimeter of the droplet for each pixel on the boundary. For the suspended droplets, diameter measurements were not taken when the average droplet diameter became less than about eight times the nominal fibre diameter because distortions of the droplet shape began to increase below this size. This could raise questions about the influence of the

fibre on the burning process when the droplet diameter becomes comparable to the fibre diameter.

For a droplet suspended from a fibre, surface tension causes liquid to be drawn up the fibre while the liquid is anchored at the fibre tip, thus stretching the liquid mass and creating a pear shape. To calculate an effective diameter of such a shape, the locations where the liquid surface changed concavity near the fibre, both at the top and at the bottom of the droplet, were excluded. Furthermore, with the highly sooting 1-chloro-octane part of the droplet boundary was sometimes obscured by the soot. This made it difficult to locate the droplet boundary. A tool in the analysis package which allowed certain regions to be 'painted' over was used to fill in the obscured portions of the droplet boundary. Although this process was obviously manual, the film records used for droplet measurements had only very small sections of the droplet boundary obscured by soot agglomerates, and thus measurement errors for this process remained negligibly small. In general, individual droplet diameter measurements had a maximum error of less than 2% (Jackson 1994).

Diameters of the luminous flame zones were measured on the movie films for some of the n-heptane and 1-chloro-octane dropelts with the image analysis package. The outer boundary of the visible luminous zone was used for the measurements. No data were taken just after ignition because of the lack of clearly defined flame boundaries. Because of the lower luminosity of the n-heptane flames and the need for reasonably strong back lighting for clear droplet images, the flame images on the high-speed movie records were not sharp enough to provide measurements of acceptable accuracy for the luminous flame zone. Images recorded on the higher light sensitivity of the CCD camera were much better, and therefore CCD images of the luminous zone for the heptane droplets presented in this study were used to measure luminous zone (i.e. flame) diameters. The highly sooting bright (yellow) flames of 1-chloro-octane, on the other hand, produced a fairly sharp image on the high-speed movie records so that 1-chloro-octane flame diameter data could be obtained from the high speed movie records.

For both fuels, soot collected in a shell-like structure (i.e. soot 'shell' as discussed in § 4) inside the flame around the droplet. Soot shell diameters were measured from the outside of the shell. The CCD video records were used for the soot shells around the n-heptane droplets and the high-speed movie records were used for soot shell diameter measurements around the 1-chloro-octane droplets. Identification of the soot shell boundary was facilitated by the painting feature of the analysis package.

The suspended droplets showed a slight indentation of the luminous zone boundary and a flattening of the soot shell around the fibre, primarily during the latter period of burning. The deviation from a spherical flame shape was not large enough to affect the measured average radius beyond the measurement uncertainties. For the soot shell measurements, the flattening of the shell near the fibre, caused by thermophoretic attraction of soot particles to the fibre, was accompanied by a slight broadening of the shell in the horizontal direction. The horizontal broadening appears to have compensated for the shrinking in the vertical direction because soot shell diameters for suspended droplets agreed well with those for unsupported free droplets of similar size.

The measurements for the luminous flame zone had an estimated maximum error of approximately 8% for the n-heptane video records and around 4% for the

1-chloro-octane film records. The maximum error for the flame measurements occur later in the droplet burning when the flame begins to shrink and the flame luminosity begins to decrease. These errors were much larger than the droplet diameter measurements because the flame boundaries were not as sharply defined and variations in the back lighting required portions of the flame boundary in some cases to be defined with the painting tool in the image analysis software. The soot shell diameters were considerably sharper, and thus their measurements were more accurate than the luminous flame zone measurements. Near the end of burning neither soot shell nor luminous flame zone measurements were taken due to the reduction in the sharpness of the soot shell boundary and to loss in flame luminosity.

4. Results and discussion

(*a*) *Evolution of droplet diameter*

Burning rate constants were obtained for n-heptane droplets with initial diameters ranging from 0.40 to 1.05 mm and for 1-chloro-octane droplets with initial diameters from 0.45 to 1.10 mm. N-heptane droplets larger than about 0.9 mm and 1-chloro-octane droplets larger than about 0.8 mm did not burn to completion during the free-fall period. None the less, for all the droplets analysed for this study, a large enough fraction of the burning period was still accessible to allow a reasonable assessment of a burning rate. The repeatability of the droplet diameter profiles for a given initial diameter range is demonstrated for n-heptane in figure 4*a* and 1-chloro-octane in figure 4*b*.

The effect of initial droplet diameter on the evolution of d^2 is illustrated in figures 5 and 6 for heptane and 1-chloro-octane, respectively. To more clearly illustrate the influence of d_0 on the burning process, the data in figures 5 and 6 were generated by interpolating d/d_0^2 values for each 0.01 increment in t/d_0^2 for all of the runs in the respective diameter ranges, and then taking the average for each initial size range. Figures 5 and 6 demonstrate the increased burning rates for the initially smaller droplets. These results stand in contrast to the spherically symmetric models mentioned in § 1 which predict that the curves for the various initial diameter ranges should be coincident when the t and d^2 are scaled with $1/d_0^2$.

Burning rate constants were found using data that corresponded to the most linear variation of d/d_0^2 with t/d_0^2 by using a least-square linear regression of the data in that region. Data from the initial period of droplet heat-up were excluded from the linear regression. This initial burning period was characterized by a slower decrease in the droplet surface area, i.e. lower burning rate. An instantaneous slope for the diameter-squared profile for a given time was approximated using the diameter measurement at that time, two measurements before and two measurements after the time of interest. When this calculated instantaneous slope began to vary about a reasonably constant value which lasted through the droplet lifetime, the heat-up period was assumed to be over. For example, heptane data in the range $0 < t/d_0^2 < 0.020$ to 0.025 were typically excluded in this process. 1-chloro-octane droplets exhibited initial heat-up periods which were around 25% longer than those of similarly sized n-heptane droplets.

The linear approximation of the data after the initial period appears to be

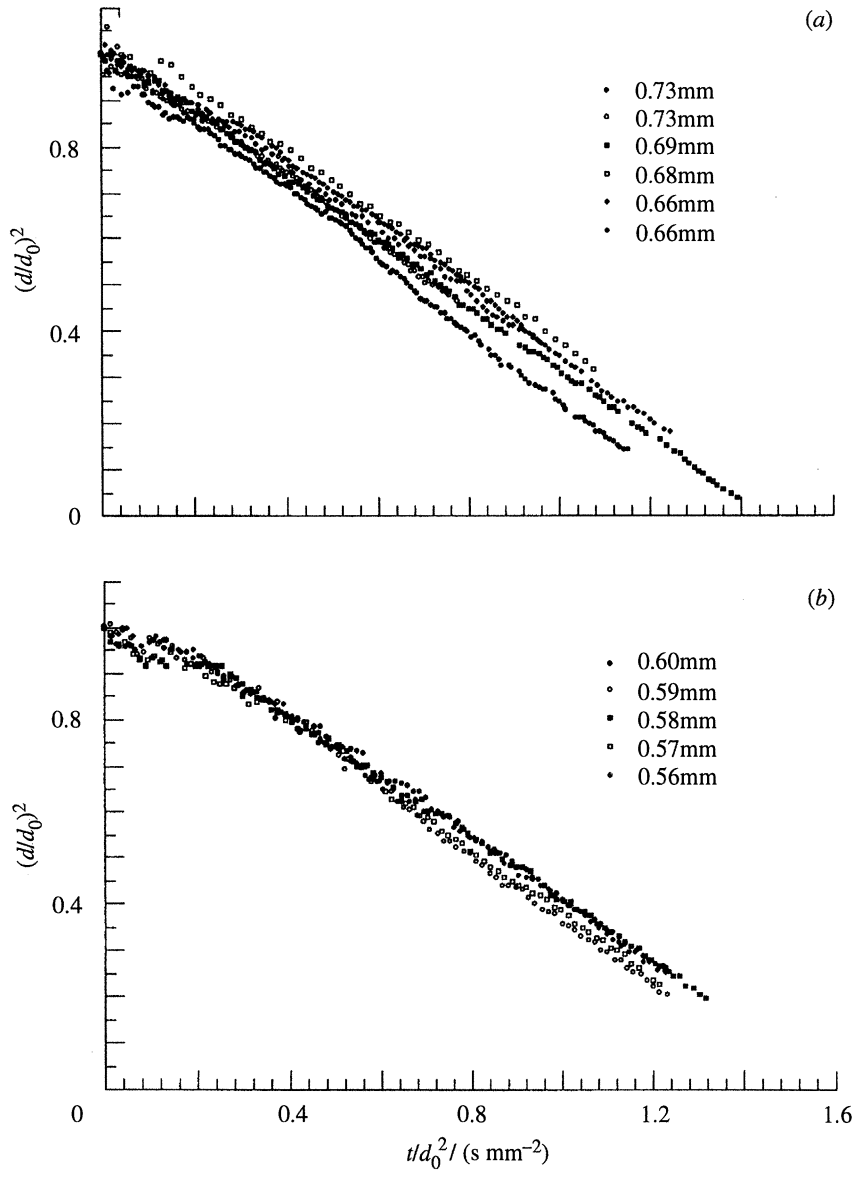

Figure 4. Sample of diameter-squared profiles for one initial diameter range: (*a*) unsupported n-heptane droplets; (*b*) fibre-supported 1-chloro-octane droplets.

accurate except with the larger 1-chloro-octane droplets as shown in figure 6. The larger 1-chloro-octane droplet diameter-squared profiles exhibited slight curvature (concave downward) which signifies a slight increase in the instantaneous K_0 as the droplet diameter decreases with time. This slight increase, of the order of 10–20%, in K_0 for the larger droplets was accompanied by a an observed decrease in the rate of soot accumulation inside the droplet and therefore may be explained in terms of less soot formation resulting in increased heat release for vaporization

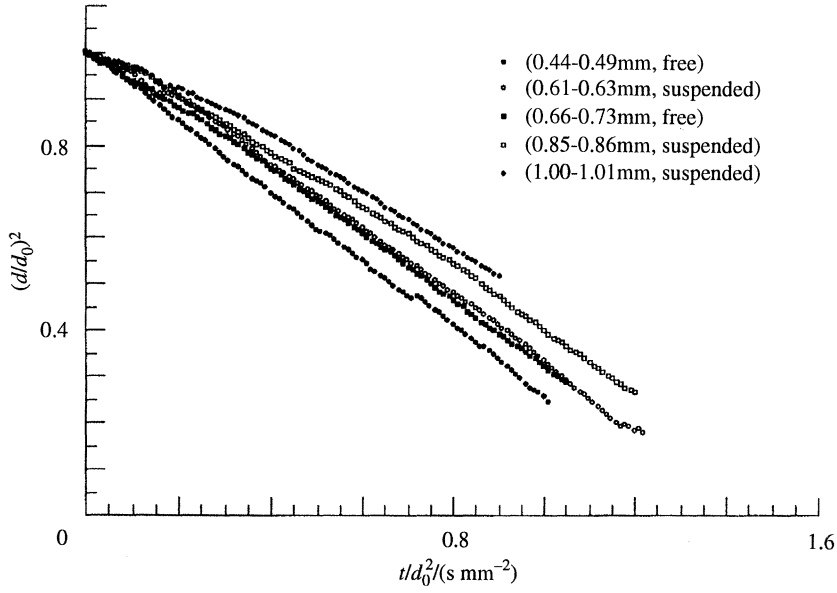

Figure 5. Averaged dimensionless diameter-squared profiles for various ranges of initial diameters for n-heptane droplets.

(cf. § 4*d*) as burning progresses. None the less, an average K_0 was still found for these larger 1-chloro-octane droplets since the curvature was slight.

The variation of burning rate constants for over 40 n-heptane droplets, both free-floating and fibre-supported, with initial diameter is illustrated in figure 7. Figure 8 shows similar data for fibre-supported 1-chloro-octane droplets. The maximum uncertainties in the burning rates were calculated from a rigorous error analysis to be in general less than 10% (Jackson 1994). Table 1 lists the burning rates grouped in the indicated initial droplet diameter ranges.

The effect of initial droplet diameter on the burning rate is clearly illustrated in figures 7 and 8, and table 1. For both fuels studied, droplets around 0.60 mm in initial diameter consistently exhibited burning rates which were more than 20% higher than those of droplets around 1.00 mm in initial diameter. The variation in burning rate with d_0 suggested that at smaller initial diameters, the decrease in burning rates with increasing d_0 was not as significant as at the larger initial diameters as shown in figures 7 and 8. As the initial diameter increased above 0.6 mm, there was a monotonic decrease in K_0 with increasing initial diameter. These trends are believed to be connected to the effect of initial droplet diameter on soot formation as discussed below.

(*b*) *Flame and soot shell diameter*

To assess flame behaviour and to determine whether quasi-steady conditions were achieved during the burning process, the evolution of flame diameters was measured for droplets of various initial diameters. The flame diameters were taken as the average of the luminous zone surrounding the droplet.

While the luminous zone boundary was taken as the boundary for the flame diameter measurements, this boundary does not necessarily correspond to the

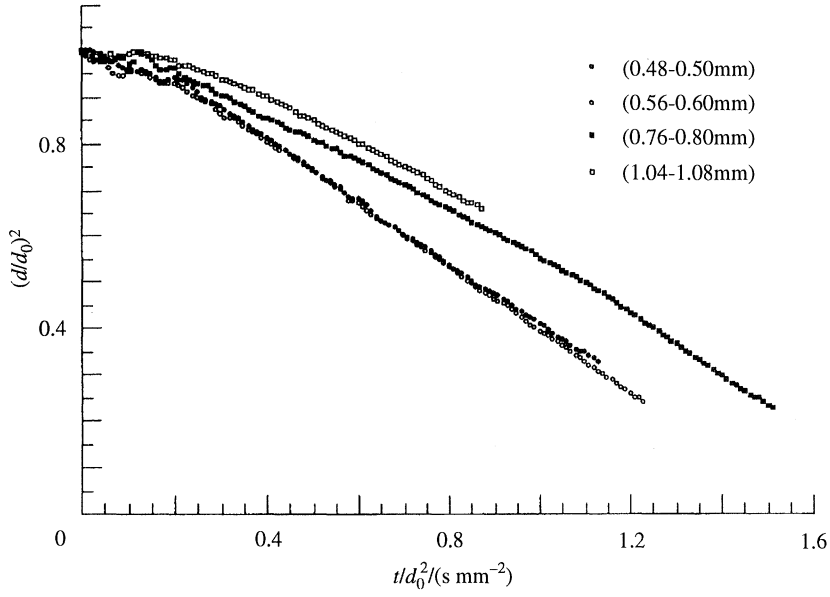

Figure 6. Averaged dimensionless diameter-squared profiles for various ranges of initial diameters for 1-chloro-octane droplets.

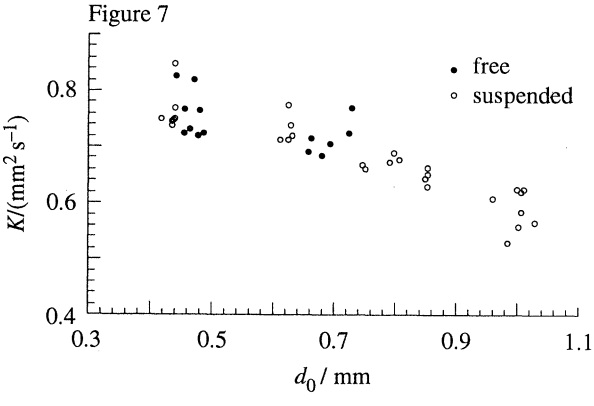

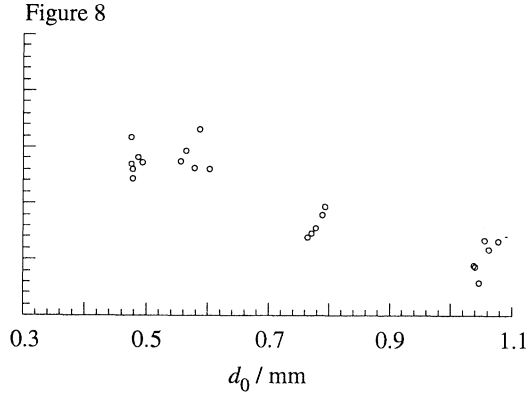

Figure 7. Burning rates against initial diameter for n-heptane droplets burning at low gravity.
Figure 8. Burning rates against initial diameter for 1-chloro-octane droplets burning at low gravity.

actual flame boundary which is defined as the location where oxidation of the fuel is completed. The luminosity arises partly from soot and soot precursor radiation, indicating that soot particles/species are in high temperature oxidative regions. Thus if the heating of the soot particles/precursors is dictated by the radial temperature profile in the gas-phase, it can be expected that the luminous zone diameter scales with the diameter of the outermost oxidation region as long as there is sufficient precursor formation. Near the end of burning when the droplet size becomes small and the flame begins to rapidly shrink, the (yellow) luminous zone also shrinks and fades. This signifies a significant reduction in soot precursor formation. When the luminous zone began to fade and lose its sharpness

Table 1. *Burning rate constants for n-heptane droplets at low gravity*

d_0 range/mm	set-up	runs	average $K/(\mathrm{mm}^2\ \mathrm{s}^{-1})$
0.42–0.45	suspended	7	0.763 (±0.038)
0.44–0.49	free-floating	8	0.758 (±0.042)
0.61–0.63	suspended	5	0.730 (±0.026)
0.66–0.73	free-floating	6	0.713 (±0.030)
0.75–0.81	suspended	5	0.671 (±0.011)
0.85–0.86	suspended	5	0.646 (±0.012)
0.96–1.03	suspended	8	0.588 (±0.035)

Burning rate constants for 1-chloro-octane droplets at low gravity

d_0 range/mm	set-up	runs	average $K/(\mathrm{mm}^2\ \mathrm{s}^{-1})$
0.48–0.50	suspended	6	0.673 (±0.025)
0.56–0.60	suspended	5	0.683 (±0.029)
0.76–0.80	suspended	5	0.561 (±0.023)
1.04–1.08	suspended	6	0.501 (±0.030)

near the end of droplet burning (such that reasonably accurate flame diameter measurements were no longer feasible), the CCD camera was able to detect a faint thin luminous (probably blue) region outside the brighter inner zone. The flame luminosity was dominated by soot radiation during the majority of the droplet burning lifetime, and therefore this faint luminous region could not be used for the flame diameter measurements.

The variation of flame stand-off ratio, d_f/d, with t/d_0^2 for n-heptane droplets are shown in figure 9. Figure 10 shows similar data for 1-chloro-octane. Droplets larger than those indicated in figures 9 and 10 were not included because their flame boundaries were too large relative to the camera field of view and could not be completely captured in the film or the CCD video images. The smallest-sized heptane droplets were also not included in the measurements because their flames and soot shells were too faint for accurate measurements. The heptane data are more sparse than the 1-chloro-octane data because the heptane measurements were taken from the CCD videos (30 frames per second resolution). The increased scatter in the heptane measurements arose from the less sharp flame boundaries of this fuel.

d_f/d for n-heptane droplets (figure 9) clearly increased as burning proceeded rather than remain constant as dictated by (2.1). This trend agreed well with more limited low-gravity data for n-heptane droplet combustion (Hara & Kumagai 1990; Chauveau & Gokalp 1990). Furthermore, the variation of d_f/d with t/d_0^2 appears to be independent of d_0 (within measurement uncertainties) for the range of d_0 shown in figure 9. This fact may suggest that characteristic times of the combustion process scale with d_0^2, but such scaling seems particularly uncertain in light of the fact that droplets of these sizes had burning rates which differed by over 15% (see table 1). These results raise questions of whether or not quasi-steady burning could be achieved in conditions under which the classical theory of spherically symmetric droplet combustion might be expected to be valid.

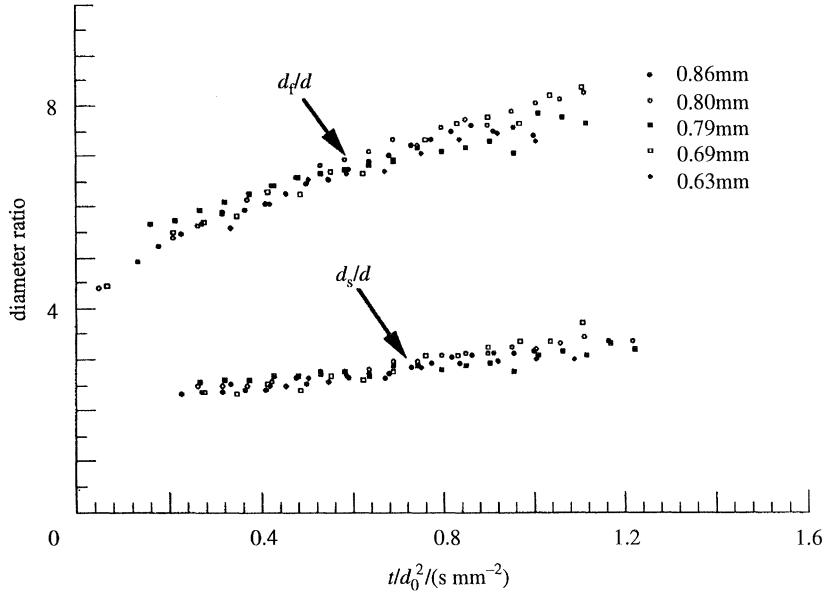

Figure 9. Flame-to-droplet diameter ratios and soot-shell-to-droplet diameter ratios for n-heptane droplets burning at low gravity.

Figure 10 shows evolution of d_f/d for 1-chloro-octane droplets. The initial droplet diameters ranged from 0.48 to 0.78 which represent initial diameter ranges for which the burning rates differed by about 20% (see table 1). These results further illustrate the independence of d_f/d on d_0 when t/d_0^2 is used for scaling. The flame stand-off ratio steadily increased from just below 4.0 in the early period of burning to around 7.5 late in the droplet burning lifetime. These values are lower than those for n-heptane (figure 9) which might be explained by the slower diffusion of fuel to the flame zone and the increased soot formation in the 1-chloro-octane.

The evolution of soot 'shell' stand-off ratios, d_s/d, are shown in figure 9 for n-heptane and figure 10 for 1-chloro-octane. The soot shell diameters remained fairly constant until late in the droplet burning lifetime when they began to decrease, although proportionately less than the droplet diameter. Currently, no theory exists to explain these results. The soot shell stand-off ratio profiles shown in figures 9 and 10 suggest that, when plotted against t/d_0^2, they are independent of d_0 for both fuels over a wide range of initial droplet diameters. This fact further suggests the scaling of characteristic times with d_0^2.

(c) *Observations of flames and soot shells*

The transient behaviour of the flame and soot for heptane and 1-chloro-octane is clearly shown in the photographic sequences of figures 11 to 13. The various photographic sequences in each figure have approximately the same progression of t/d_0^2 values to provide a basis for comparison between them (the corresponding times after ignition are given in parenthesis below each photograph). Although visible differences exist between the combustion of the two fuels in this study,

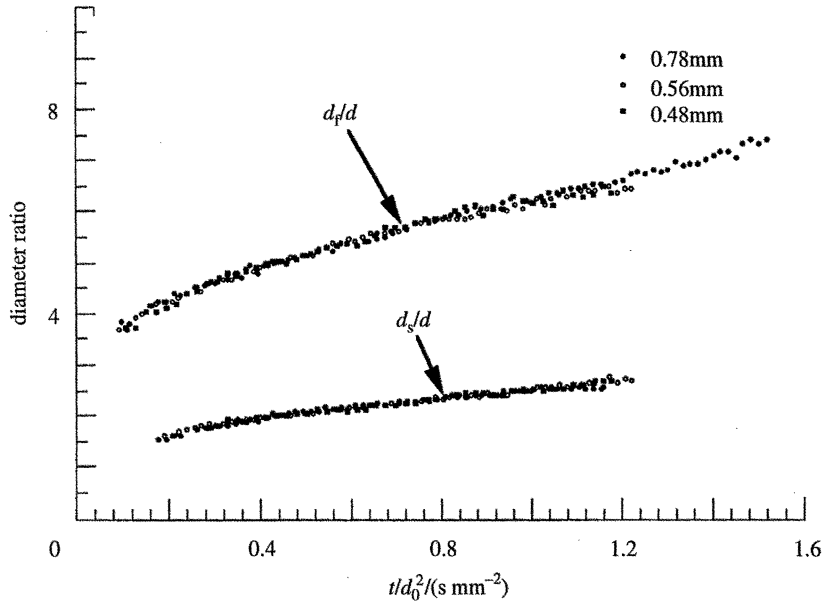

Figure 10. Flame-to-droplet diameter ratios and soot-shell-to-droplet diameter ratios for 1-chloro-octane droplets burning at low gravity.

particularly the increased sooting and flame luminosity for 1-chloro-octane, both fuels exhibit common trends in the development of the soot shell and the flame.

Early in the burning process when the flame is expanding, soot begins to form just inside the flame boundary for both fuels as discussed in § 4*b*. If the growth of the particles becomes large enough such that thermophoretic forces overtake outward inertia created from the Stefan flow, the particles are pushed inward before they reach the oxidation region of the flame. Where the thermophoretic forces balance the outwardly directed drag forces due to the Stefan flow, a shell-like structure forms. While the perimeter of the shell suggests that it was a contiguous structure as shown in some of the views in figure 11, in reality it was quite porous and consisted of individual agglomerates suspended in a well-defined zone – the 'shell' – around the droplet. It should be noted that spherical soot shells are clearly visible in the photographs originally reported by Okajima & Kumagai (1975) for free n-heptane droplets burning in microgravity, but they were not discussed. As burning progressed the location of the shell did not change significantly relative to the droplet diameter (see figures 9 and 10) and the soot particles began to agglomerate into larger units. This agglomeration was more evident for the denser soot shells of the 1-chloro-octane flames in comparison to the n-heptane flames. The large soot agglomerates are eventually pushed out away from the droplet and into the flame zone because the outward drag force increases more rapidly with agglomerate size than does the thermophoretic force (Jackson *et al.* 1992). These trends are demonstrated in the photographic sequences of figure 11, 12, and 13 with the exception of the smallest n-heptane droplet in figure 12 ($d_0 = 0.44$ mm) which produced a very minimal amount of soot.

The soot agglomerates generally escaped the flame without complete oxidation implying a loss in heat generation due to unoxidized carbon. As the agglomerates

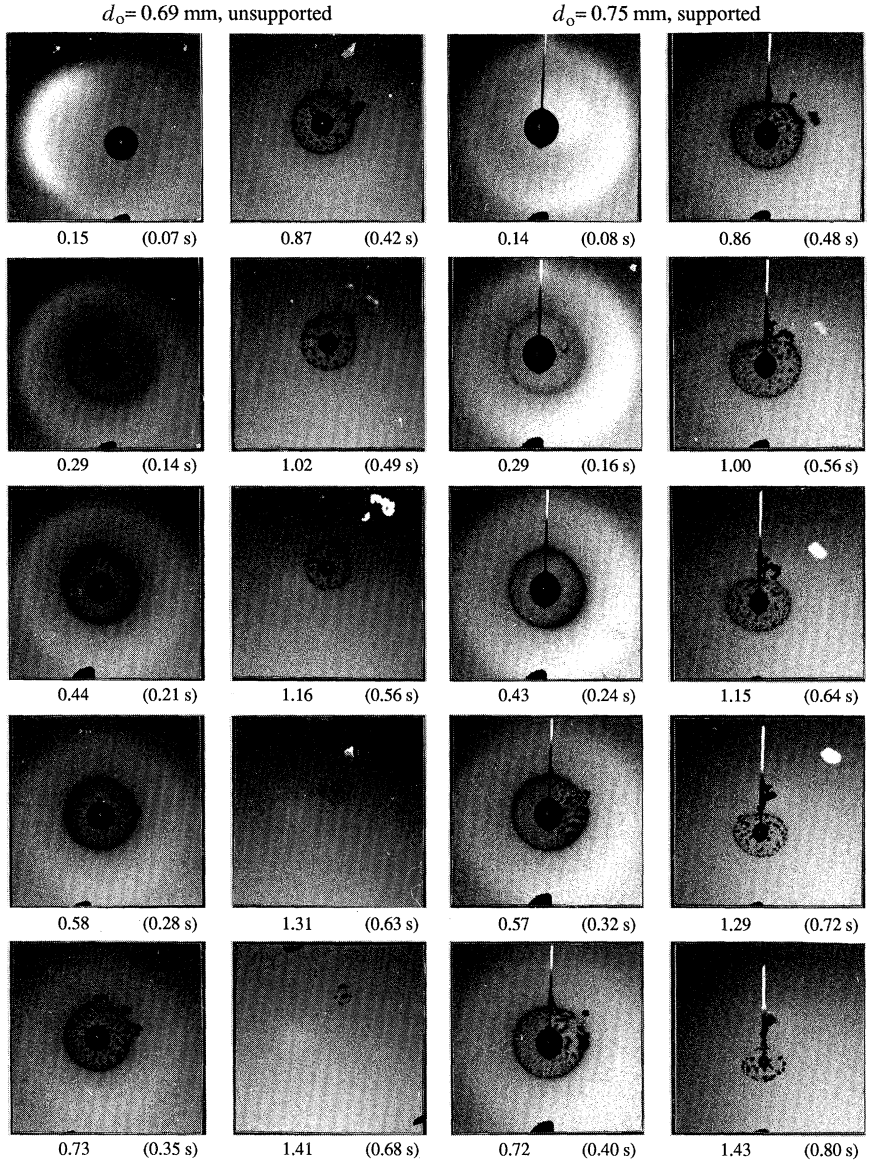

Figure 11. Comparison of two photographic sequences of unsupported and fibre-supported n-heptane droplets with similar initial diameters. Values of t/d_0^2 (in s mm^{-1}) are given beneath each sequence.

left the shell, the shell became less dense. Fewer particles were added to the flame later in the droplet's lifetime, perhaps because the flame began to contract and overtake soot precursors before particles could grow large enough to experience thermophoretic forces which pushed them inward (Randolph & Law 1986). Near the end of vaporization, the soot shell also began to contract inward until the end of burning. As vaporization was completed, the contracting flame overtook the soot shell and disrupted the remaining soot structure as shown in the last frame of the unsupported droplet sequence in figure 11.

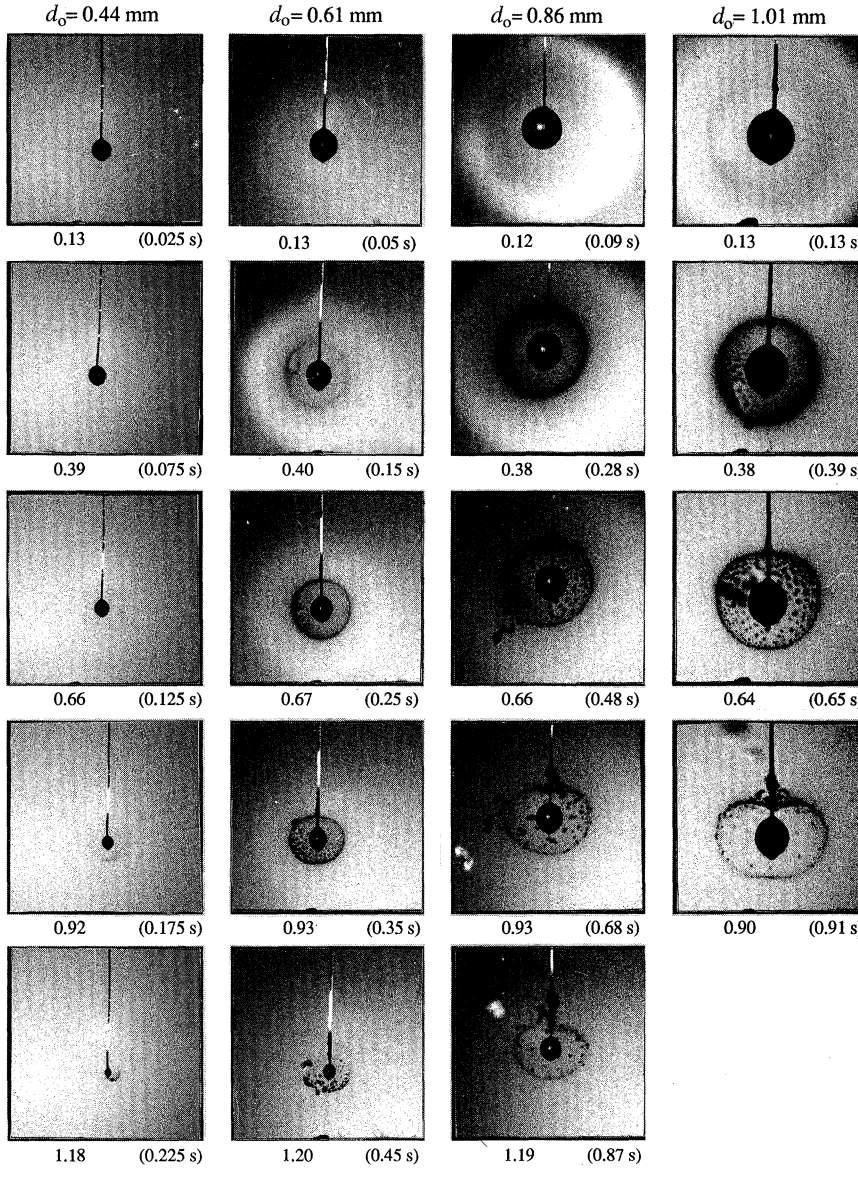

Figure 12. Comparison of four photographic sequences of fibre-supported n-heptane droplets with different initial diameters. Values of t/d_0^2 (in s mm^{-1}) are given beneath each sequence.

Figure 11 shows two photographic sequences of n-heptane droplets burning at low gravity: one unsupported droplet with $d_0 = 0.69$ mm and one suspended droplet with $d_0 = 0.75$ mm. The trends in the development of the soot shell mentioned above, as well as the emission of soot agglomerates and the reduction in flame luminosity, are demonstrated by both sequences. Both droplets burned to completion but the unsupported droplet, being slightly smaller, had a 5% higher burning rate constant than the fibre-supported droplet shown (see table 1). None of the droplets for which complete burning could be observed appeared

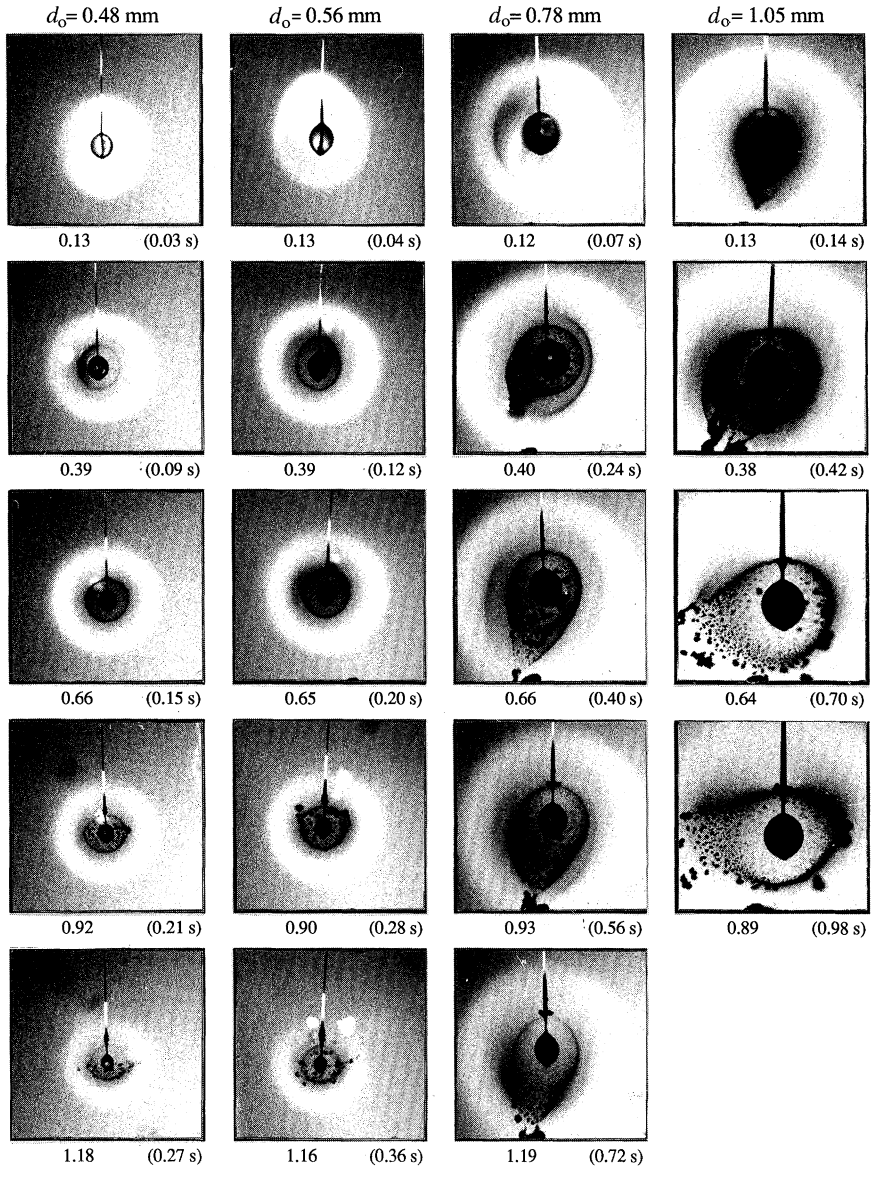

Figure 13. Comparison of four photographic sequences of fibre-supported 1-chloro-octane droplets with different initial diameters. Values of t/d_0^2 (in s mm^{-1}) are given beneath each sequence.

to extinguish. However, almost all, including the smallest droplets, left small soot agglomerates from the collapse of the soot shell at the end of burning. It was possible for these agglomerates to be mistaken for remaining liquid.

The fibre-supported droplet sequence in figure 11 reveals some interactions between the fibre and soot particles. The fibre appears to attract soot agglomerates which has been attributed to thermophoresis (Randolph & Law 1986). This collection on the fibre forced the soot shell to move down the fibre as combustion proceeded and caused it to become less spherical. Dimensionless soot shell

equivalent diameters for fibre-supported droplets agreed well with those for unsupported droplets (cf. figure 9) because the reduction in the vertical diameter of the shell around the fibre-suspended droplet was accompanied by a broadening in the horizontal direction of the soot shell.

The changes in soot formation and flame luminosity with initial droplet diameter for n-heptane are demonstrated in the four photographic sequences of fibre-supported n-heptane droplets in figure 12. Although the lighting is slightly different for the four sequences, the differences in soot and flame intensity for different droplet sizes are clearly apparent. The last picture in the sequence of the largest droplet in figures 12 and 13 ($t/d_0^2 = 1.20\ \mathrm{s\ mm^2}$) is not shown because the free-fall was terminated before the burning process was completed.

The reduction in the density of the soot shell with increasing time occurred for the larger droplets because they rapidly formed large agglomerates which left the shell and broke through the flame. The smallest droplet ($d_0 = 0.44$ mm), on the other hand, did not appear to show any soot shell formation until near the end of burning. The increase in the soot shell density is also slower for the $d_0 = 0.61$ mm droplet than the larger droplets.

Figure 13 shows similar trends for 1-chloro-octane droplets, though with denser soot shells and more luminous flames than heptane. Even the smaller droplets (e.g. $d_0 = 0.48$ mm) show luminous flames and comparatively rapid soot shell development. The more rapid soot formation for the chlorinated alkane may be attributed to the increased fuel pyrolysis initiated by the C–Cl bond breaking in the regions between the droplet and the flame (McKinnon & Howard 1990). Initially larger droplets develop thick soot shells and large agglomerates much more rapidly than initially smaller droplets as is evident by scanning any row in figure 13. The rapid formation of soot in the larger droplets causes a shell to form even during the early heat-up period of the combustion process. During this time, vaporization rates and the outwardly directed drag forces are apparently low which results in thermophoresis pushing the soot shell in very close to the droplet (e.g. $t/d_0^2 = 0.13\ \mathrm{s\ mm^2}$ in figure 13).

The increase in the density of the soot shell structure for the larger 1-chloro-octane droplets resulted in rapid formation of large agglomerates which broke out of the shell and through the flame. These agglomerates often grow large enough through surface reactions and coagulation such that the spherical nature of the shell is distorted when the agglomerates break out. This effect is illustrated in figure 13 for the droplets with $d_0 = 0.78$ mm and 1.05 mm. The removal of these agglomerates resulted in a significant decrease in the soot shell density as combustion proceeded and may have further decreased soot formation due to the lower surface area of soot particles. This fact may explain the slight increases in the burning rate constants later in the droplet lifetime of the larger 1-chloro-octane droplets as evidenced by the curvature in the d^2 plots in figure 6.

(*d*) *Effects of soot formation on burning rates*

Since the development of the 'd^2-law' (Spalding 1953) which has served as a basis for interpreting droplet combustion phenomena, timescales in droplet combustion have been assumed to scale as $1/d_0^2$. This scaling is based upon K_0 (1.1) being independent of the initial droplet diameter. Soot formation is neglected in the development which leads to this result. For the sooting fuels examined in the present study, the dimensionless droplet diameter profiles for different droplet

sizes are not coincident when plotted against t/d_0^2 as illustrated in figures 5 and 6. Rather, the asymptotic burning rates in the so-called 'steady-burning' régime decrease with increasing initial diameter. On the other hand, the dimensionless soot shell positions and flame boundaries for various droplet sizes appear to be independent of d_0 when plotted against t/d_0^2 (see figures 9 and 10).

The photographs in figures 12 and 13 suggest that the amount of soot collected in the shell and unoxidized by the flame is a more sensitive function of the initial droplet diameter than the d_0^2 dependence. The smallest n-heptane droplets showed almost no collection of soot inside the flame, and the low flame luminosity suggests minimal soot oxidation. An increase by a factor of two in the initial droplet diameter led to the formation of a thick soot shell around the droplet (cf. figure 12) and to emission of large soot agglomerates during burning.

The effect of soot on the burning rate constant should be traceable to heat transferred from the flame to the droplet. The soot shell could act as a barrier for heat transfer in the gas-phase back to the droplet. The soot shell can also act as a barrier by radiating heat away from the droplet. Concerning conduction heat transfer, soot does have a higher heat capacity than the surrounding gas phase molecules and thus would have tended to reduce thermal diffusion back to the droplet. However, this heat capacity should be offset by the higher thermal conductivity of soot relative to the surrounding gases. Therefore, increased soot concentrations in the larger droplet flames most likely did not significantly affect the ability for heat to diffuse back to the droplet.

A more probable mechanism to account for reduced heat transfer between the flame and droplet with increased sooting may be the reduction of fuel oxidation in the flame zone. The soot shell may act as a physical barrier for mass diffusion of molecules, or cause fuel molecules to react on the surface of the soot particles particles before reaching the oxidation zone. A reduction in the mass flux of fuel species to the flame would reduce the chemical heat release from the oxidation zone and thereby result in lower heat flux to the droplet for vaporization and thus a lower burning rate. If the soot was eventually oxidized, much of its stored energy would be liberated as heat available to the droplet. However, figures 11 to 13 showed significant amounts of soot remaining inside the flame and eventually escaping the flame unoxidized.

Because the most rapid means of soot formation is surface growth to newly formed soot particles, and because soot particles encourage fuel pyrolysis (Haynes & Wagner 1981), there can be an autocatalytic effect in soot formation. This may contribute to the sensitivity of sooting in the droplet flames with respect to initial droplet diameter. The residence times of fuel molecules in the high temperature regions between the droplet and the flame may be scaled as d^2 (Jackson *et al.* 1992). Therefore, with larger droplets, more time is available for fuel pyrolysis and soot formation. A large amount of soot formation early in the combustion process of large droplets may encourage further soot formation by surface reactions on hot newly formed soot particles. As the initial droplet size is increased, proportionately less carbonaceous molecules reach the flame for oxidation and proportionately more form soot. If the amount of soot formed is a more sensitive function of droplet diameter than d^2, then the absolute amount of fuel being transferred to the flame is not exactly proportional to d^2 or the surface area of the droplet. For larger d^2, then, a higher fraction of vaporized fuel goes

into forming soot which reduces the proportionate amount of heat released for droplet vaporization. This leads to a lowering of the burning rate constant.

5. Conclusions

The present experimental results clearly showed that K decreases with increasing initial droplet diameter for two sooting fuels: n-heptane and 1-chloro-octane. Qualitative assessment of the film records of the combustion process for both fuels showed that soot accumulation inside the droplet flame increases significantly with initial droplet diameter. These trends suggest that soot accumulation may lower the droplet burning rates.

A balance of thermophoretic and Stefan flow drag forces on soot particles inside the droplet flame leads to the formation of a shell-like structure of soot agglomerates around the droplet. The soot shell may retard the burning rate by acting as a chemical sink reducing the fuel mass flux to the flame and perhaps as a shield for heat transfer from the flame to the droplet. The impact of the soot shell on heat and mass transfer should increase with the density of the soot shell formed around the droplet. The density of the soot shell increases dramatically with initial diameters ranging from 0.4 to 1.0 mm. Carbon atoms have longer gas-phase residence times inside the flames of larger droplets, and these longer residence times are conjectured to allow for more soot precursors to form, soot particles to nucleate, and agglomerates to grow by surface reactions and coagulation. The associated increase in soot formation with longer residence times of fuel molecules inside the flames may explain the reduction in K_0 for the larger droplets.

Soot formation can significantly affect the global performance parameters of diffusion flames (e.g. K_0) for even supposedly lightly sooting fuels such as n-heptane. The simplicity of spherically symmetric (microgravity) flames may allow for the testing of models with complex chemical kinetics which incorporate soot formation. These models may then be refined to analyse more complex diffusion flames that characterize practical devices such as incinerators or industrial gas turbines.

The authors gratefully acknowledge the support of the National Aeronautics and Space Administration through Grant no. NAG 3-987 and the New York State Center for Hazardous Waste Management (Dr Ralph R. Rumer, Director). G.S.J. was also supported by a NASA Graduate Student Researcher Program fellowship.

References

Avedisian, C. T., Yang, J. C. & Wang, C. H. 1988 On low gravity droplet combustion. *Proc. R. Soc. Lond.* A **420**, 183–200.

Chauveau, C. & Gökalp, I. 1990 Experiments on the burning of n-heptane droplets in reduced gravity. In *Proc. Seventh European Symp. Mat. Sci. and Fluid Physics in Microgravity*, pp. 467–472.

Choi, M. Y., Dryer, F. L. & Haggard, J. B. Jr 1990 Observations on a slow burning régime for hydrocarbon droplets: n-heptane/air results. In *Proc. 23rd Symp. (Int.) Comb.*, pp. 1597–1604. Pittsburgh: The Combustion Institute.

Choi, M. Y., Dryer, F. L., Green, G. J. & Sangiovanni, J. J. 1993 Soot agglomeration in isolated, free droplet combustion. Paper no. 93-0823, 31st Aerospace Sciences Meeting, Reno, Nevada, January 11–14.

Fendell, F. E., Sprankle, M. L. & Dodson, D. S. 1966 Thin-flame theory for a fuel droplet in slow viscous flow. *J. Fluid Mech.* **26**, 267–280.

Gogos, G., Sadhal, S. S., Ayyaswamy, P. S. & Sundararajan, T. 1986 Thin-flame theory for the combustion of a moving liquid drop: effects due to variable density. *J. Fluid Mech.* **171**, 121–144.

Hara, H. & Kumagai, S. 1990 Experimental investigation of free droplet combustion under microgravity. In *Proc. 23rd Symp. (Int.) Comb.*, pp. 1605– 1611. Pittsburgh: The Combustion Institute.

Haynes, B. S. & Wagner, H. Gg. 1981 Soot formation. *Prog. Energy Comb. Sci.* **7**, 229–273.

Jackson, G. S. 1994 Spherically symmtetric droplet combustion of sooting and multi-component fuels. Ph.D. thesis, Cornell University, Ithaca, New York.

Jackson, G. S., Avedisian, C. T. & Yang, J. C. 1991 Soot formation during combustion of unsupported methanol/toluene mixture droplets in microgravity. *Proc. R. Soc. Lond.* A **435**, 359–369.

Jackson, G. S., Avedisian, C. T. & Yang, J. C. 1992 Observations of soot during droplet combustion at low gravity: n-heptane and monochloro-alkane mixtures. *Int. J. Heat Mass Trans.* **35**, 2017–2033.

Kesten, A. S., Sangiovanni, J. J. & Goldberg, P. 1980 Conceptual experimentation of gas phase particulate formation in gas turbine combustors. *J. Engng Power* **102**, 613–618.

Law, C. K. 1976 Unsteady droplet combustion with droplet heating. *Comb. Flame* **26**, 219–233.

Law, C. K. & Williams, F. A. 1972 Kinetics and convection in the combustion of alkane droplets. *Comb. Flame* **19**, 393–405.

Matalon, M. & Law, C. K. 1985 Gas-phase transient diffusion in droplet vaporization and combustion. *Comb. Flame* **59**, 213–215.

McKinnon, J. T. & Howard, J. B. 1990 Application of soot formation model: effects of chlorine. *Comb. Sci. Technol.* **74**, 175–197.

Monaghan, M. T., Siddall, R. G. & Thring, M. W. 1968 The influence of initial diameter on the combustion of single drops of liquid fuels. *Comb. Flame* **12**, 45–53.

Okajima, S. & Kumagai, S. 1975 Further investigations of combustion of free droplets in a free falling chamber including moving droplets. In *Proc. 15th Symp. (Int.) Comb.*, pp. 401–407. Pittsburgh: The Combustion Institute.

Puri, I. K. & Libby, P. A. 1991 The influence of transient oroperties on droplet burning. *Comb. Sci. Technol.* **76**, 67–80.

Randolph, A. L. & Law, C. K. 1986 Influence of physical mechanisms on soot formation and destruction in droplet burning. *Comb. Flame* **64**, 267–284.

Spalding, D. B. 1953 The combustion of liquid fuels. In *Proc. 4th Symp. (Int.) Comb.*, pp. 847–864. Pittsburgh: The Combustion Institute.

Williams, A. 1973 Combustion of droplets of liquid fuels: a review. *Comb. Flame* **21**, 1–31.

Williams, F. A. 1985 *Combustion theory*, pp. 52–91. Menlo Park: Benjamin Cummings.

Yang, J. C., Jackson, G. S. & Avedisian, C. T. 1990 Combustion of unsupported methanol/dodecanol mixture droplets at low gravity. In *Proc. 23rd Symp. (Int.) Comb.*, pp. 1619–1625. Pittsburgh: The Combustion Institute.

Received 26 July 1993; accepted 9 February 1994

(a)

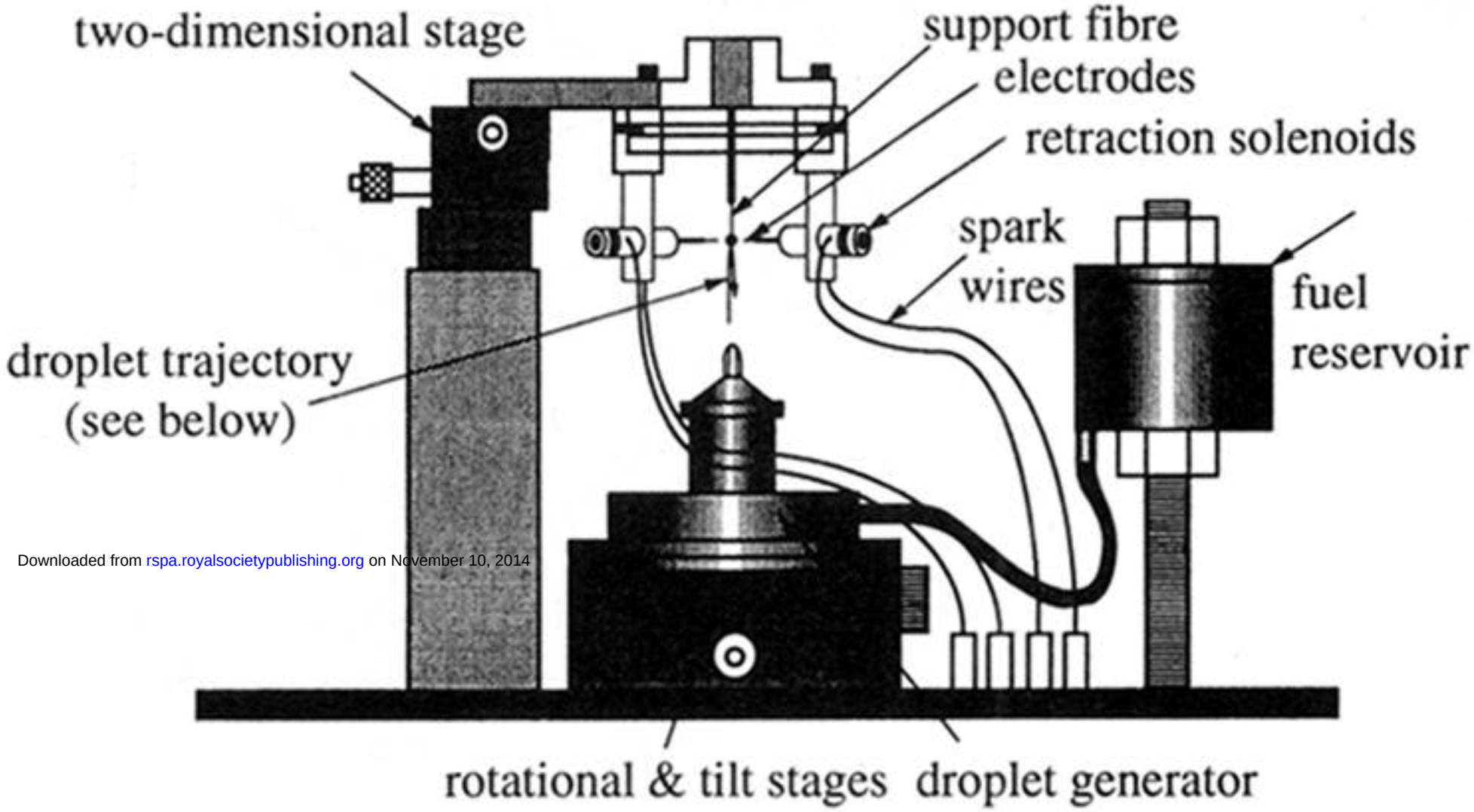

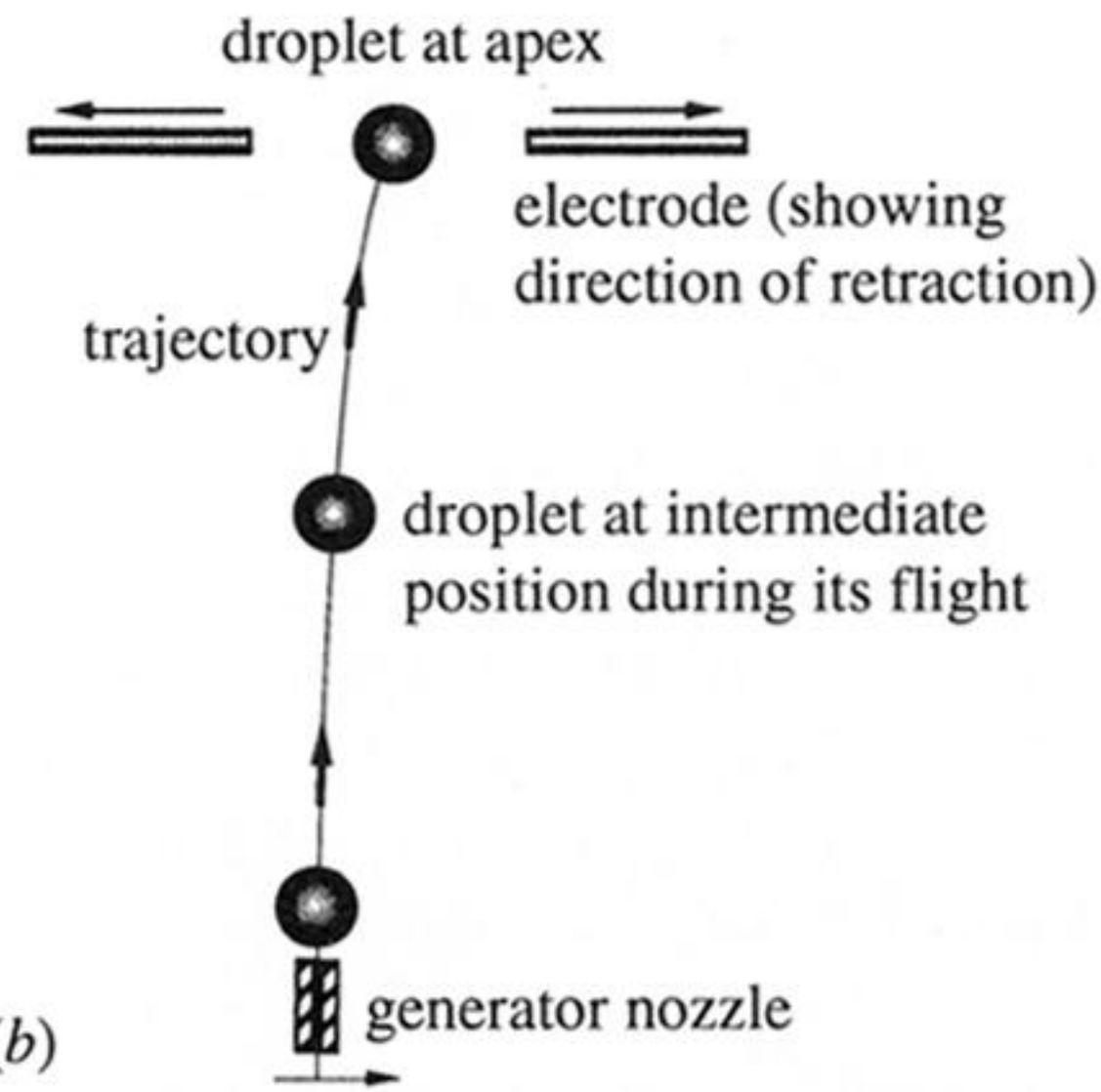

(b)

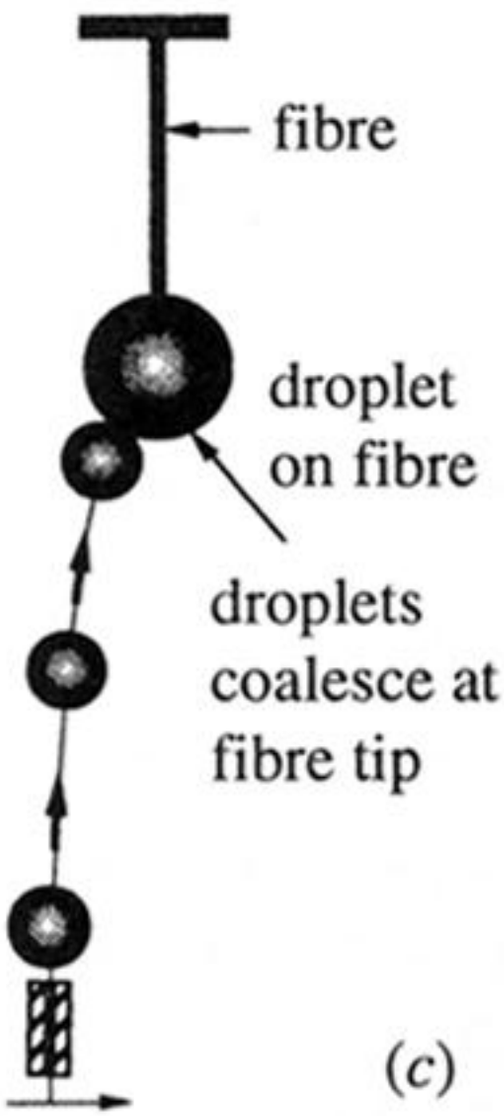

(c)

Figure 2. (*a*) Droplet generator with electrode mount. (*b*) Illustration of free droplet arrangement. (*c*) 'Shooting' method for forming a small droplet on a fibre.

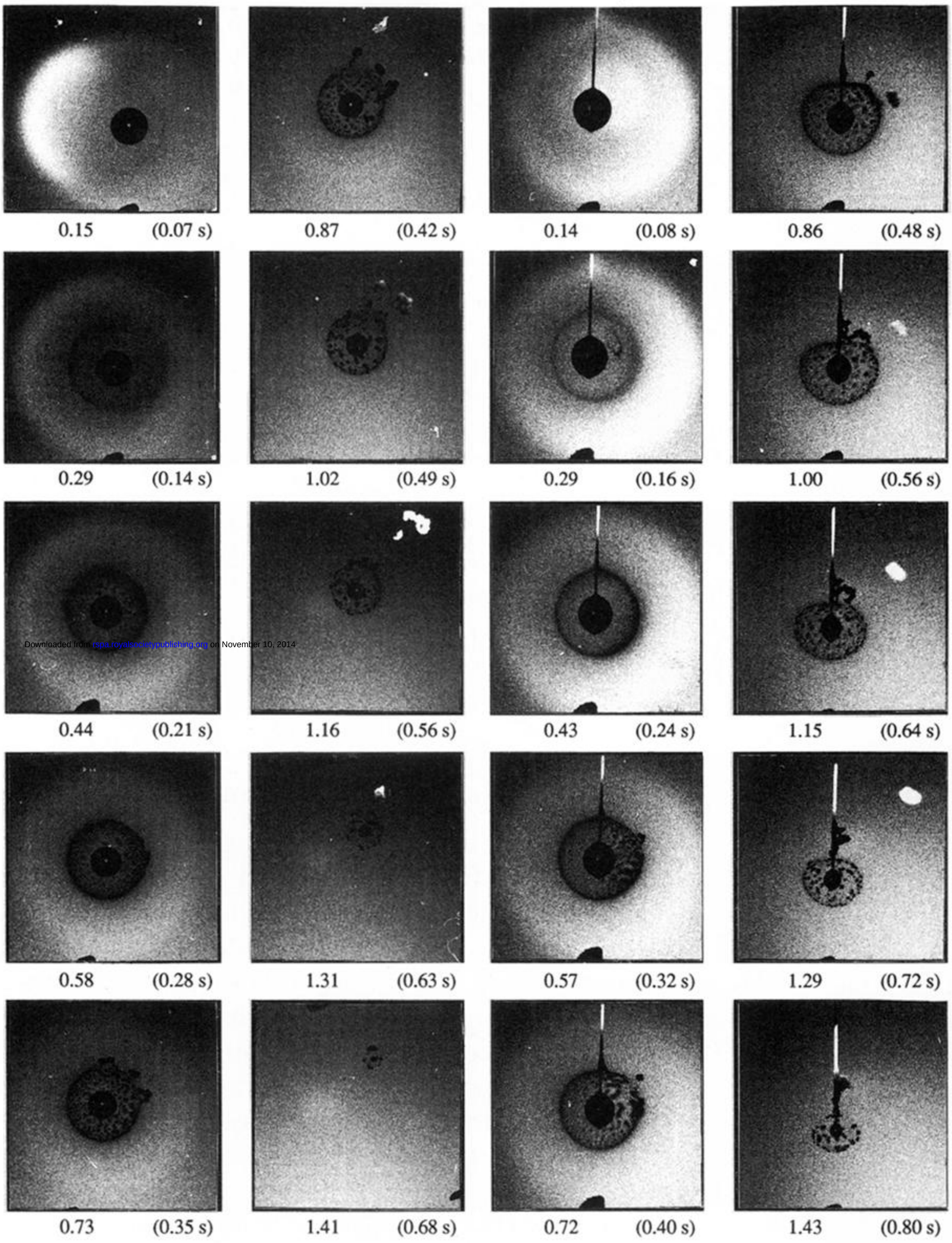

Figure 11. Comparison of two photographic sequences of unsupported and fibre-supported n-heptane droplets with similar initial diameters. Values of t/d_0^2 (in s mm^{-1}) are given beneath each sequence.

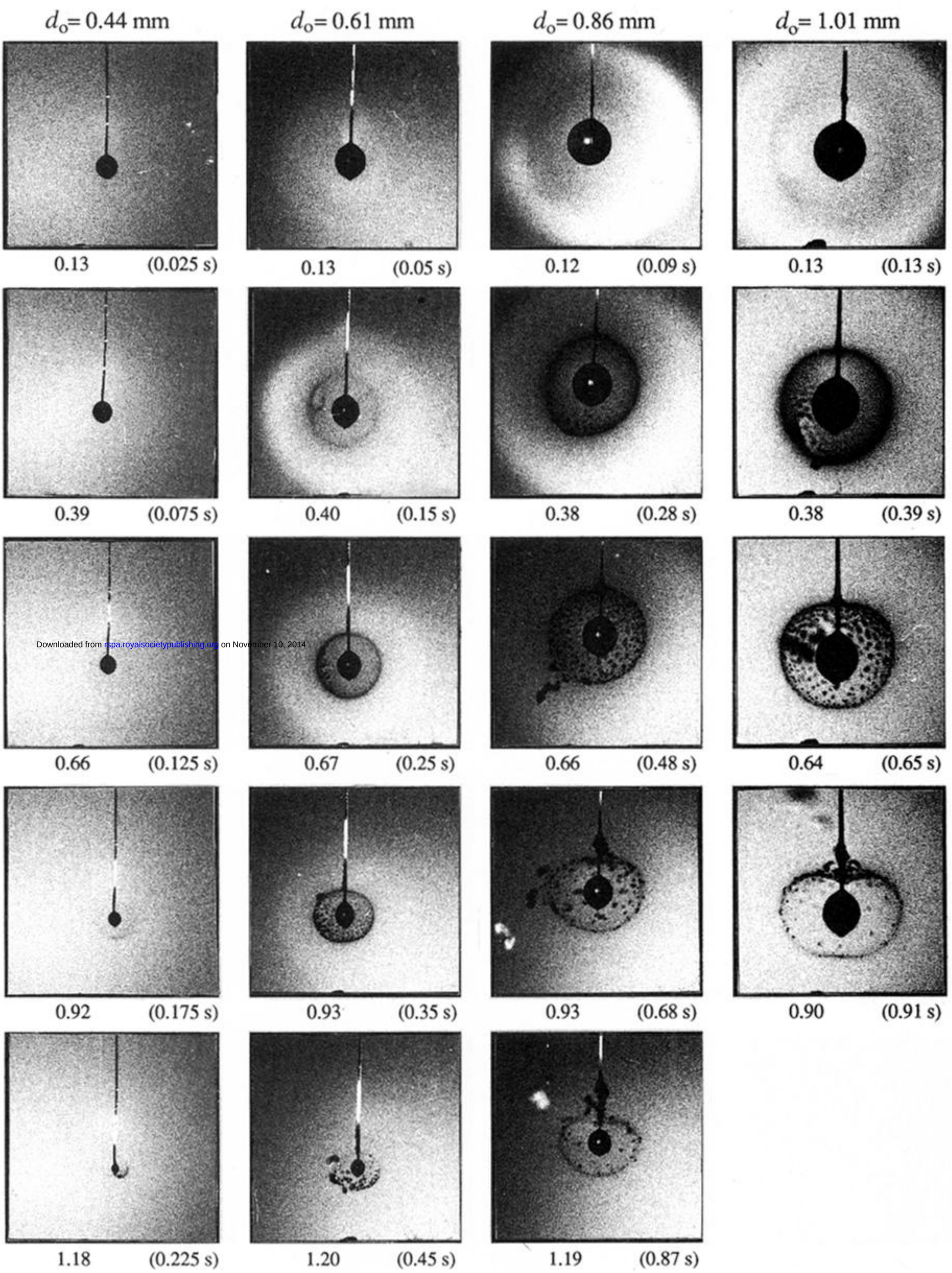

Figure 12. Comparison of four photographic sequences of fibre-supported n-heptane droplets with different initial diameters. Values of t/d_0^2 (in s mm^{-1}) are given beneath each sequence.

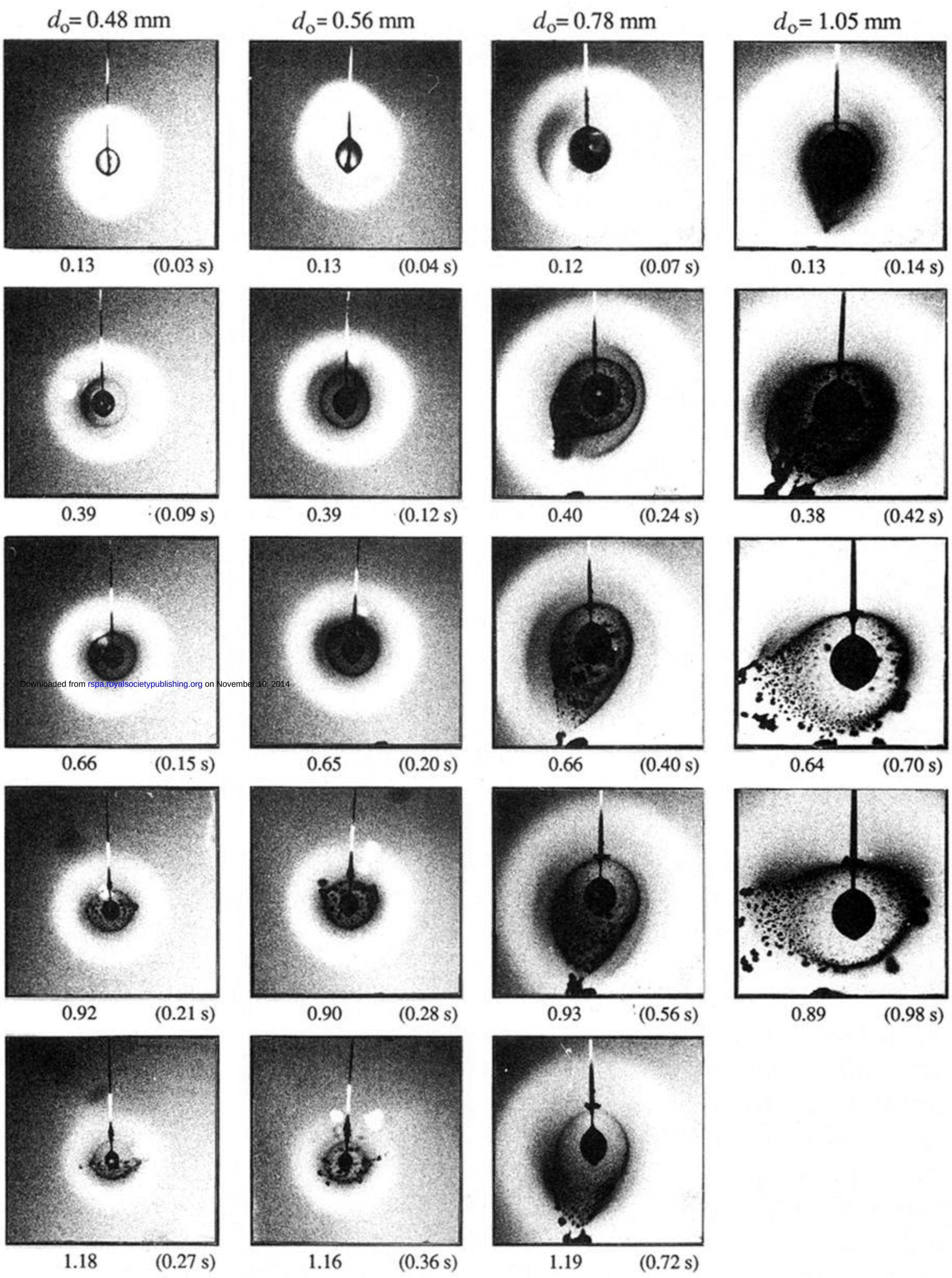

Figure 13. Comparison of four photographic sequences of fibre-supported 1-chloro-octane droplets with different initial diameters. Values of t/d_0^2 (in $\mathrm{s\,mm^{-1}}$) are given beneath each sequence.